

## Supporting Information

### Selective photoelectrocatalytic oxidation of 3-methylpyridine to vitamin B<sub>3</sub> by WO<sub>3</sub> decorated nanotube-structured TiO<sub>2</sub>

Sıdıka Çetinkaya<sup>a</sup>, Levent Özcan<sup>b</sup>, Oğuzhan Alagöz<sup>c</sup>, Leonardo Palmisano<sup>d</sup> and Sedat Yurdakal<sup>\*a</sup>

<sup>a</sup>Kimya Bölümü, Fen-Edebiyat Fakültesi, Afyon Kocatepe Üniversitesi, Ahmet Necdet Sezer Kampüsü, 03200 Afyonkarahisar, Turkey.

<sup>b</sup>Biyomedikal Mühendisliği Bölümü, Mühendislik Fakültesi, Afyon Kocatepe Üniversitesi, Ahmet Necdet Sezer Kampüsü, 03200 Afyonkarahisar, Turkey.

<sup>c</sup>Kimya Mühendisliği Bölümü, Mühendislik Fakültesi, Afyon Kocatepe Üniversitesi, Ahmet Necdet Sezer Kampüsü, 03200 Afyonkarahisar, Turkey.

<sup>d</sup>Schiavello-Grillone Photocatalysis Group, Università degli Studi di Palermo, Dipartimento di Ingegneria (DI), Viale delle Scienze, 90128 Palermo, Italy.

\*Corresponding author e-mail: [sedatyurdakal@gmail.com](mailto:sedatyurdakal@gmail.com)

#### S 1. Experimental part

##### S1.1. Preparation of Ti plates

Ti plates with dimensions of 5.0 cm x 8.0 cm x 0.10 cm (width x length x thickness) were smoothed out with sandpaper of different grades (400, 600, 800, 1000, 1200, and 1500) (Yurdakal et al., 2020). Then, they were cleaned in an ultrasonic bath (Bandelin Sonorex) for 10 minutes with acetone, ethanol, and distilled water, respectively, and chemically treated with a solution containing 4% HF, 31% HNO<sub>3</sub>, and 65% water by mass. Finally, cleaning was done in an ultrasonic bath in pure water for 10 minutes and drying at room temperature.

##### S1.2. Preparation of nanotubes structured TiO<sub>2</sub> on Ti plates

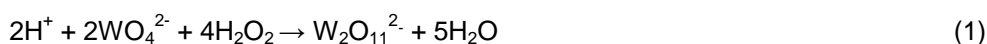
2% (v/v) water, 98% (v/v) ethylene glycol solution and NH<sub>4</sub>F (to obtain a concentration of 0.3% by mass) were mixed to carry out the anodic oxidation process using two-electrode system (Fig. S1) (Çetinkaya 2022). A constant potential at 32V for different times (from 15 min to 5h) was used for the immersed Ti plates in the electrolyte solution under a constant mixture speed (200 rpm) to obtain low crystalline, mainly amorphous TiO<sub>2</sub> nanotubes on Ti plates (Yurdakal et al. 2020). All the prepared electrodes were calcined in an oven (Protherm, PLF-110/10) at 500 °C for 3h in an air atmosphere (temperature increase rate: 3 °C/min) to crystallize the TiO<sub>2</sub>. The electrodes are named NT-yh, in which NT denotes nanotube, and y hours of applied potential.



**Fig. S1.** Two-electrode system in which the anodic oxidation process is applied for nanotube-structured TiO<sub>2</sub> production on a Ti plate.

### S1.3. Preparation of WO<sub>3</sub> decorated nanotubes structured TiO<sub>2</sub> on Ti plates

The prepared NT-4h electrode was modified by immersing it in a cell containing 0.50, 1.0, or 2.0 mM Na<sub>2</sub>WO<sub>4</sub> in the presence of 1.0 mM H<sub>2</sub>SO<sub>4</sub> and 10 mM H<sub>2</sub>O<sub>2</sub> solution. A Pt sheet (2 cm x 2 cm) was used as the counter electrode. Then, potential scanning between -0.75 and +0.75 V (toward Ag/AgCl) was repeated ten times at a scanning rate of 50 mV s<sup>-1</sup> (Davaslıoğlu et al., 2021). The modification reactions were given in eq. 1 and 2 (Martins et al. 2017). In the NT-4h-"z" WO<sub>3</sub> electrode code, "z" indicates the concentration (mM) of Na<sub>2</sub>WO<sub>4</sub> solution used for decorating. Another "NT-4h-1WO<sub>3</sub>" plate was calcined (at 500 for 3h) after preparation and named as NT-4h-1WO<sub>3</sub>-500.



### S1.4. Characterization Experiments

An X-ray diffraction (XRD) diffractometer (Bruker, D8 Advance Model) with Cu K $\alpha$  radiation (1.544 Å) was used to determine the crystal phases of TiO<sub>2</sub> on the plates. The electrodes were analysed directly.

Scanning Electron Microscope (SEM) images were performed with a FEI NanoSEM 650 model device. The electrodes were analysed directly without covering them with a thin film of gold. SEM images were taken using a Through Lens Detector (TLD). EDX mapping was also applied for some samples by means of the EDX detector coupled with the SEM system.

Photocurrent performances of photoanodes were determined chronoamperometrically under UVA and visible irradiation. The electrolytic medium in which the photocurrent values were determined was the same one in which the PEC selective oxidation experiments were performed (see Section S1.5).

The electronic states of the elements of sample's surfaces were determined by means of X-ray Photoelectron Spectroscopy (XPS, SpecsLab, Germany) with monochromatic Al K $\alpha$  (1486.6 eV) radiation, using an electron flood gun in high vacuum (10<sup>-9</sup> Torr). The binding energy values of the spectra were calibrated with C1s = 284.6 eV. The samples, taken from the plate surface with a spatula,

were supported on carbon adhesive type before the analyses. The raw signals were also analyzed by using CasaXPS software.

### *S1.5. Photoelectrocatalytic Experiment System*

In addition to the PEC experiments, photocatalytic (with light, no potential) and electrocatalytic (with potential, under dark) experiments were also carried out for comparison purposes. In homogeneous experiments were performed only using the substrate solutions (no catalyst and no bias) in the same set-up used for PEC system.

Photoelectrocatalytic and electrocatalytic experiments were carried out in a three-electrode electrochemical system connected to a computer-controlled potentiostat-galvanostat (Ivium, Vertex model) device (Fig. S2). Ti/TiO<sub>2</sub> photoanodes were used as working electrodes, a Ti plate as the counter electrode, and Ag/AgCl electrode as a reference electrode in the system. A 5 cm x 5 cm portion of the photoanodes and 4 cm x 5 cm portion of Ti plate were immersed in the solution.

Experiments were carried out with different light sources. Three 8W UVA fluorescent lamps with a maximum wavelength of 365 nm were used as the light source for the UVA irradiation. For UV-Vis irradiation, a 100 W tungsten lamp was used in a water cooling jacket present in a reactor. To obtain only visible light, 1 M NaNO<sub>2</sub> was filled into the reactor in the same system used for the UV-Vis system because 1 M NaNO<sub>2</sub> absorbs only the UV part of the beam, exhibiting a practical and inexpensive filter behaviour (see Fig. S2b (Tek et al., 2015)).

The PEC experimental setup is shown in Fig. S2 for the cases where the UVA and UV-Vis (or Vis) light are turned off and on, respectively. The distance between the photoanodes and the light source is positioned as close as possible: 4.5 cm for UVA and 3 cm for UV-Vis or Vis sources. Homogeneous oxidation system under UVA and UV-Vis (or Vis) used for photolytic oxidation of 3-methylpyridine is also shown in Fig. S3.

Irradiation intensity values of the used lamps were determined with a radiometer (Deltaohm, DO9721) with probes measuring between 315-400 nm and 400-1050 nm. The values are reported in Table S1.

Before starting the experiment, the PEC system was stirred for 10 minutes (in the dark and without applying potential) to bring the system to thermodynamic and adsorption/desorption equilibria. Then the experiment was started, and the mixing process (at 400 rpm) continued throughout the experiments.

The experiments were carried out in environmentally friendly conditions, where water was used as the solvent and oxygen in the air (or water) as the oxidant. The solution in contact with the atmosphere provided oxygen from the air, and no oxygen gas was sprayed into the system. Thus, our experiments were carried out practically and economically. The initial concentration of 3-methylpyridine was 0.5 mM, and Na<sub>2</sub>SO<sub>4</sub> was used as the electrolyte. Experiments were carried out with 150 mL of 3-methylpyridine solution in a borosilicate glass beaker used as a reactor.

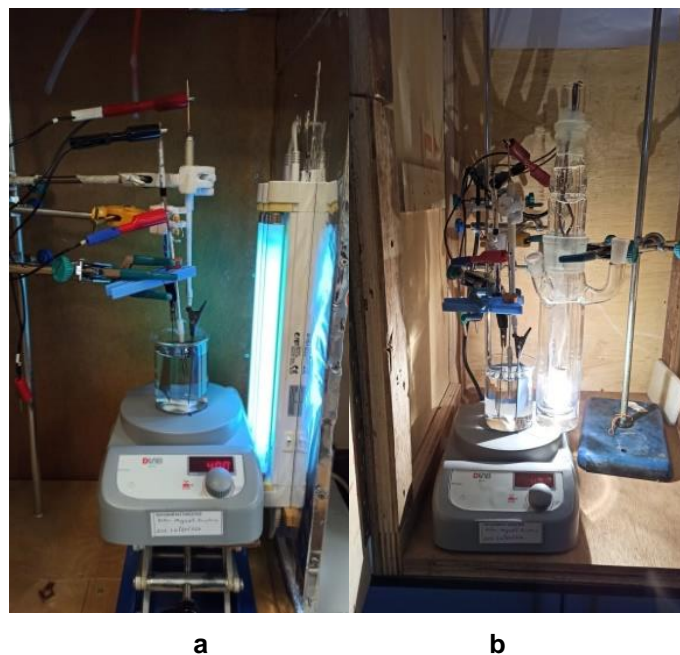


**Fig. S2.** The PEC system applied for oxidation of 3-methylpyridine under UVA (a) and UV-Vis (or Vis) (b).



**Fig. S3.** Homogeneous oxidation system under UVA (a) and UV-Vis (or Vis) (b) used for photolytic oxidation of 3-methylpyridine.

### S1.6. Analytical Techniques

Qualitative and quantitative analyses of samples taken from electrocatalytic, photocatalytic and PEC experiments were performed with High Performance Liquid Chromatography (HPLC, Shimadzu, Prominence model, SPD-M20A DAD detector) equipped with a column (Synchronis C-18) held at 303 K. Retention times of the substrate, intermediates and products to be analysed along with their UV-Vis

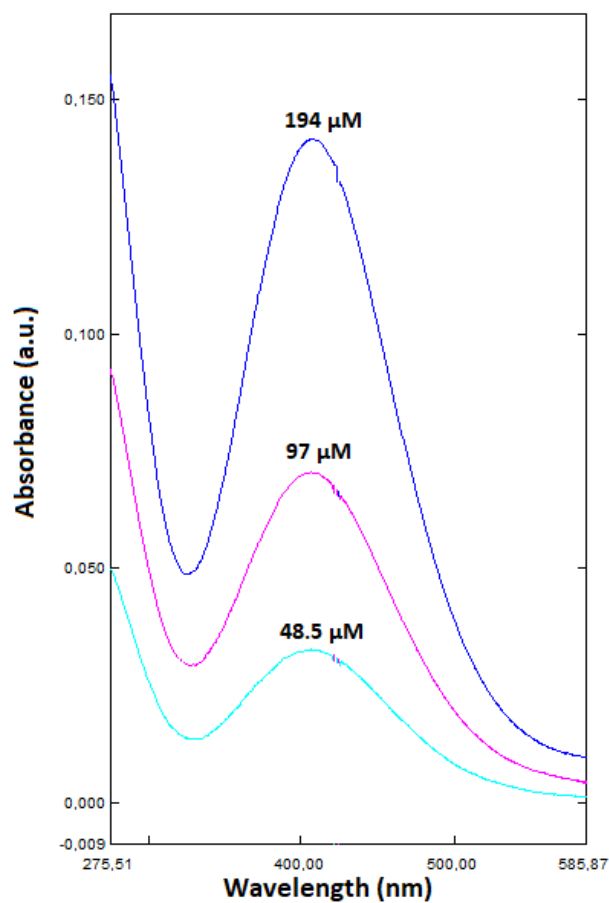
spectra were compared with those of known standards (Sigma-Aldrich, purity  $\geq 98\%$ ). The mobile phase was an aqueous solution of methanol (40%, v/v) with a flow rate of  $0.4 \text{ cm}^3 \cdot \text{min}^{-1}$ .

Total Organic Carbon analyses were performed with a Shimadzu TOC (TOC-LCPN model) device to determine the amount of carbon dioxide resulting from mineralization. The carbon (inorganic and organic) concentrations (as ppm) were determined as  $\text{CO}_2$  in an FT-IR detector (inside the instrument) after processing the samples at ca  $680 \text{ }^\circ\text{C}$  in the presence of air. Then, the concentrations of inorganic carbon were determined by titration with 2 M HCl in the same instrument. The differences of the two analyses above described gave the concentration of carbon derived from mineralized organic species. Consequently, the results obtained using the initial samples and those obtained with samples taken after a certain time during the PEC experiments corresponded to the concentrations of carbon derived from the mineralization of organic species throughout the runs. The concentrations (as mM) are the same as those of  $\text{CO}_2$ , but it is worth noting that they are reported divided by 6 in the tables of this paper (the carbon atoms of substrate) for the stoichiometric normalization.

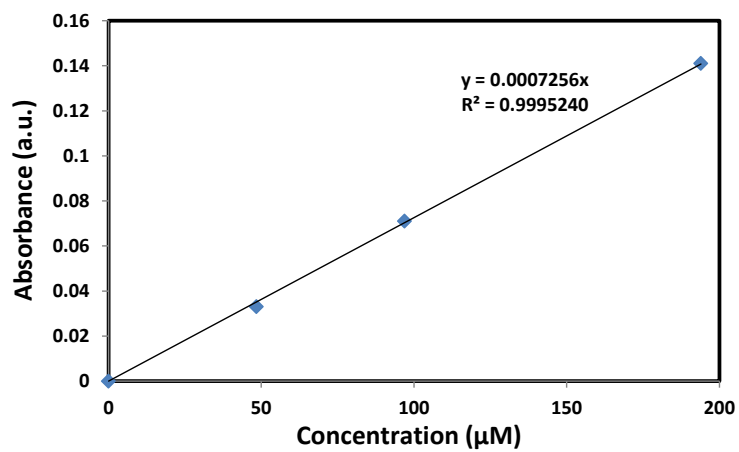
Some HPLC and TOC analyses have been repeated; the experimental error resulted less than 2%.

$\text{NH}_4^+$ ,  $\text{NO}_2^-$ , and  $\text{NO}_3^-$  analyses at the end of homogeneous and photoelectrocatalytic experiments were performed using an ion chromatography (ICS-5000<sup>+</sup> THERMO) equipped with an anionic (A519) and cationic (A619) columns.

In order to determine the amount of  $\text{H}_2\text{O}_2$ , initially, we prepared  $\text{TiOSO}_4$  solution by adding 30 mg  $\text{TiO}_2$  (anatase, Hombikat) in concentrated  $\text{H}_2\text{SO}_4$  (20 mL) in a beaker. The magnetically stirred suspension was then heated on a hot plate until a clear solution was obtained.  $\text{TiOSO}_4$  could be complexed with  $\text{H}_2\text{O}_2$ , which gives an absorbance at ca. 405 nm. Therefore,  $\text{H}_2\text{O}_2$  amount could be analysed using the spectrophotometric method using a UV Spectrophotometer (Shimadzu, UV-1800) (Amin and Olson 1967; Gökdere et. al., 2019). We prepared a calibration curve (See Fig. S4) and determined the  $\text{H}_2\text{O}_2$  amounts for the 0.5, 1, and 3 h reaction times (See Fig. S5).



(a)



(b)

**Fig. S4.** (a) The spectrum of different concentrations of  $\text{H}_2\text{O}_2$  in the presence of excess amount of  $\text{TiOSO}_4$ . (b) The calibration curve of absorbance versus different concentration of  $\text{H}_2\text{O}_2$  in the presence of excess amount of  $\text{TiOSO}_4$ .

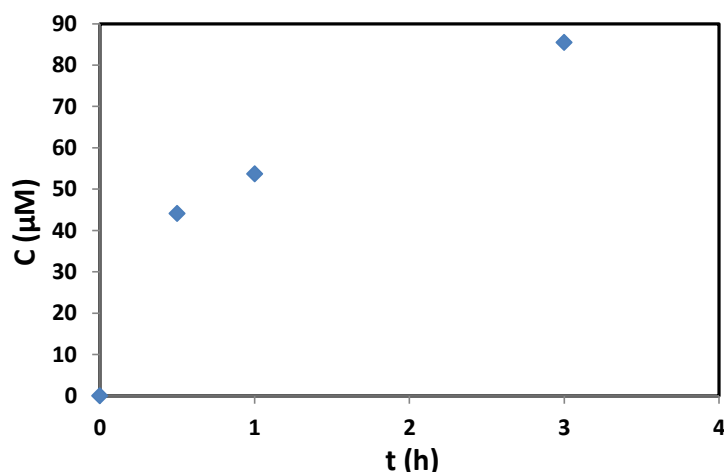


**Fig. S5.** H<sub>2</sub>O<sub>2</sub> concentration values of a PEC run using NT-4h-1WO<sub>3</sub> versus time. Applied potential: 0.5 V, pH 7, [Na<sub>2</sub>SO<sub>4</sub>] = 5 mM. Excess amount of TiOSO<sub>4</sub> was added in the sample before spectrophotometric analyses.

The formation selectivity (%) and substrate conversion (%) of the products are formulated below (eq. 3 and 4):

$$\% \text{ Selectivity} = (\text{Amount of product formed, mmol}) / (\text{Amount of substrate reacted, mmol}) \times 100 \quad (3)$$

$$\% \text{ Conversion} = (\text{Amount of substrate reacted, mmol}) / (\text{Amount of initial substrate, mmol}) \times 100 \quad (4)$$

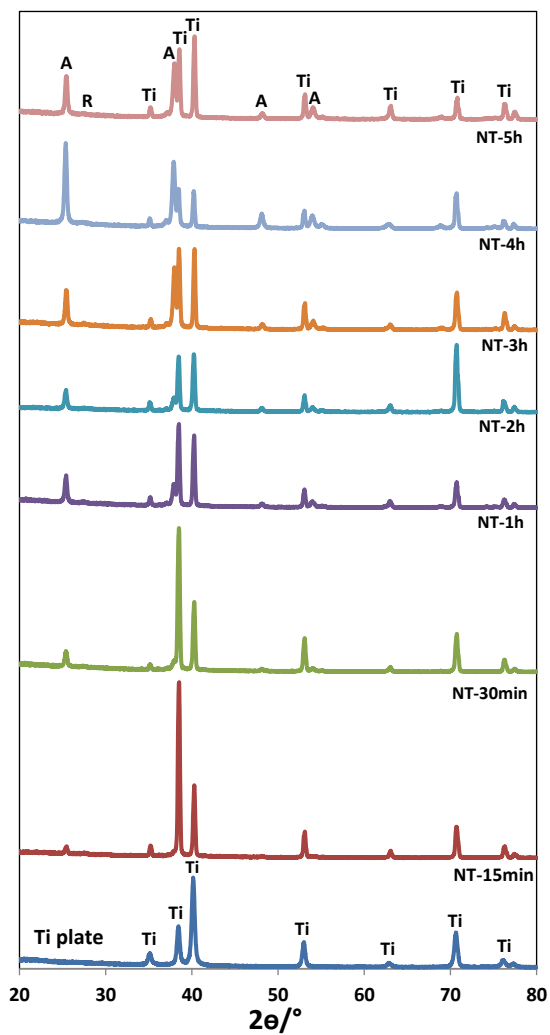
### S1.7. Kinetic calculations

Using the data obtained from HPLC and TOC analyses of samples taken from the reaction medium at different times, the selectivity and conversion value of each product (including CO<sub>2</sub>), the initial oxidation rate of 3-methylpyridine (-r<sub>0</sub>) and the values of the first order rate constant (k) were calculated.

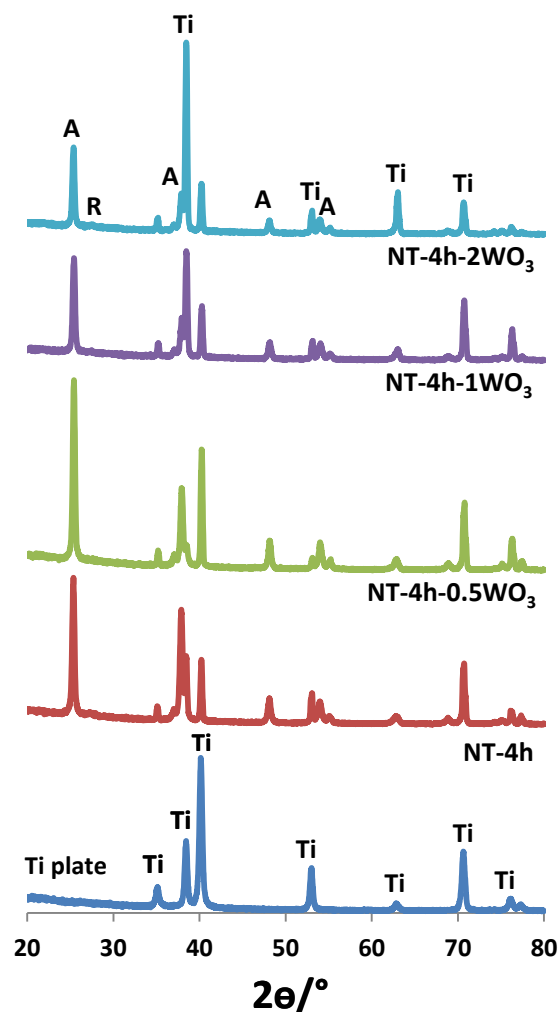
## S2. Characterization section of “Results and discussion”

Fig. S6 and S7 show the X-ray diffraction (XRD) patterns of the plates. The peak values at 2θ = 25.58°, 38.08°, 48.08° and 54.58° correspond to the anatase phase, those at 2θ = 27.5°, 36.5°, 41.0°, 54.1° and 56.5° to the rutile phase and those at 2θ = 34.95°, 38.25°, 40.05° and 52.90° to metallic Ti (Yurdakal et al. 2020). All the TiO<sub>2</sub> present on the plates are mainly in the anatase phase with some traces of rutile. Since the TiO<sub>2</sub> structures present on the Ti plates are in the form of thin films, all XRD diffractograms also include metal plate patterns. By increasing the anodic oxidation time to produce the nanotube structure, the intensity of the XRD peaks generally increased. After 4 hours of anodic oxidation, however, the intensity of the XRD peaks decreased again. This was probably due to the formation of various pieces formed by fracture of the TiO<sub>2</sub> film and the unordered structure that was produced after a long time of anodic oxidation. Average primary particle size (calculated by the Scherrer equation) of the anatase phase of the electrodes was approx. 35 nm (Table S2). XRD diffractograms of

WO<sub>3</sub>-decorated Ti/TiO<sub>2</sub> samples were also performed (see Fig. S7). However, no peaks belonging to WO<sub>3</sub> were detected, probably due to the negligible amount of this oxide compared to both TiO<sub>2</sub> and metallic titanium.



**Fig. S6.** XRD patterns of Ti plate and nanotube structured TiO<sub>2</sub> on Ti plates by anodic oxidation method for different times (from 15 min to 5h). A: Anatase, R: Rutile, Ti: metallic titanium.



**Fig. S7.** XRD patterns of  $\text{WO}_3$  decorated nanotube structured  $\text{TiO}_2$  on Ti anodes. A: Anatase, R: Rutile, Ti: metallic titanium.

The  $\text{TiO}_2$  nanoparticles on the Ti surface have a nanotube structure, as can be seen in Fig. S8. By increasing the anodic oxidation time (15 min to 5h) applied to nanotube preparation, the inner diameter of the nanotube increases (30 to 50 nm), and the nanotube wall thickness decreases (23 to 10 nm) (see Table S2). On the other hand, the  $\text{TiO}_2$  surface of the NT-5h electrode has an irregular nanotube/nanowire structure as the upper shell is almost completely broken due to the long-term applied anodic oxidation (Fig. S8). EDX analysis proved the presence of W on the  $\text{TiO}_2$  surface, and mapping analysis proved that W is homogeneously distributed (Fig. S9). In addition, with the increase of W salt concentration used for W decorating, the amount of W on the  $\text{TiO}_2$  surface also increased.

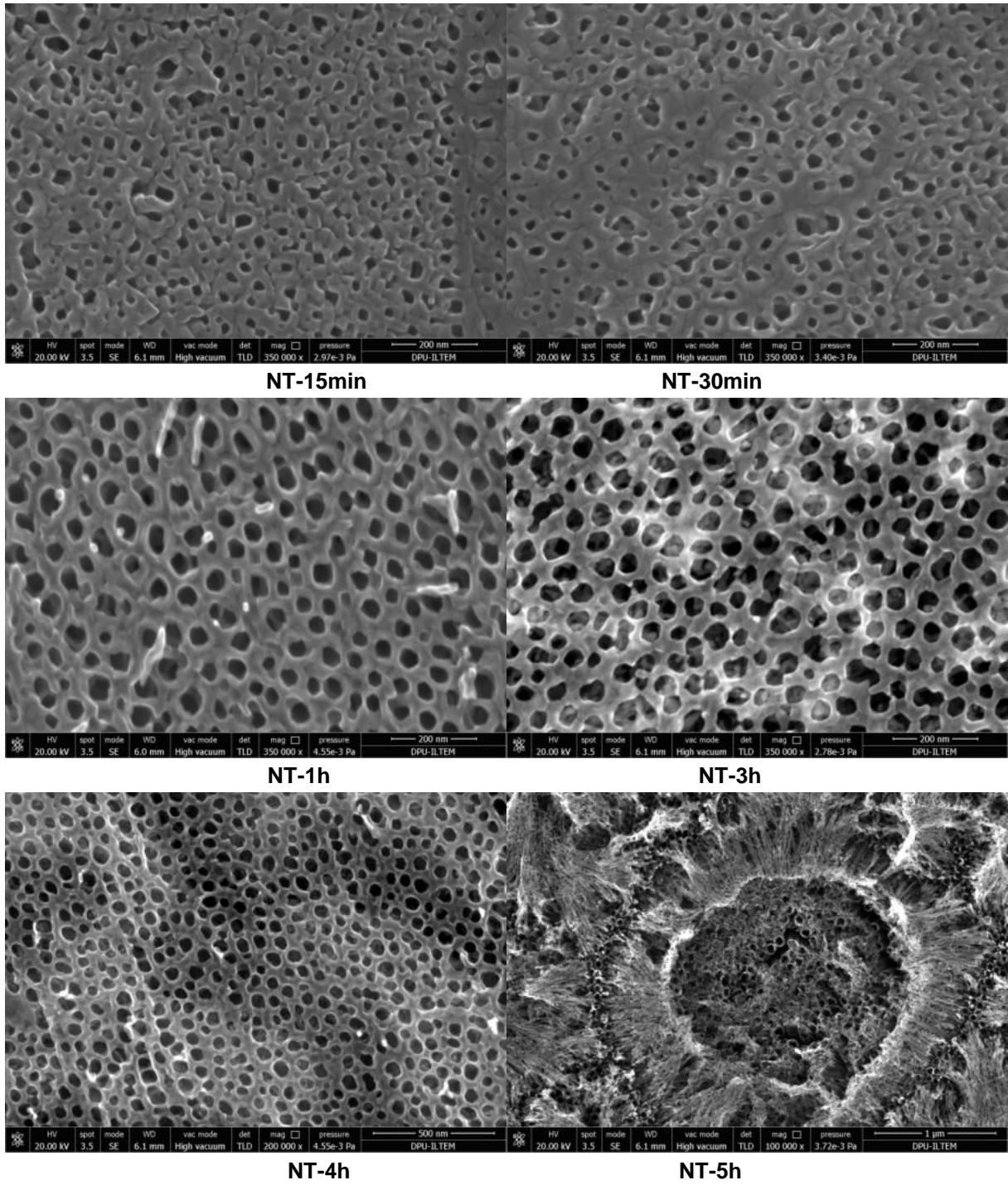
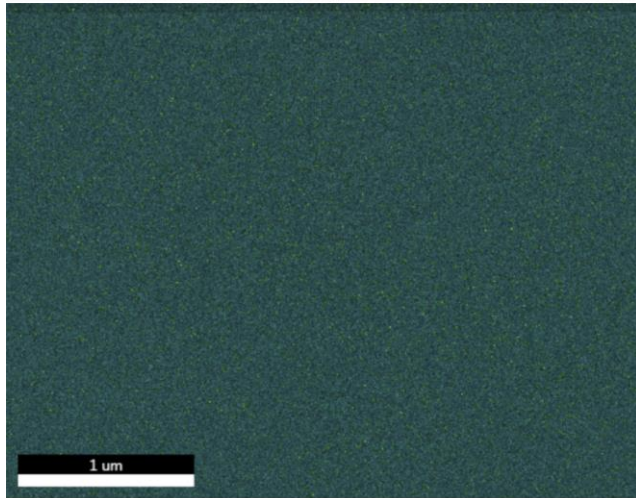
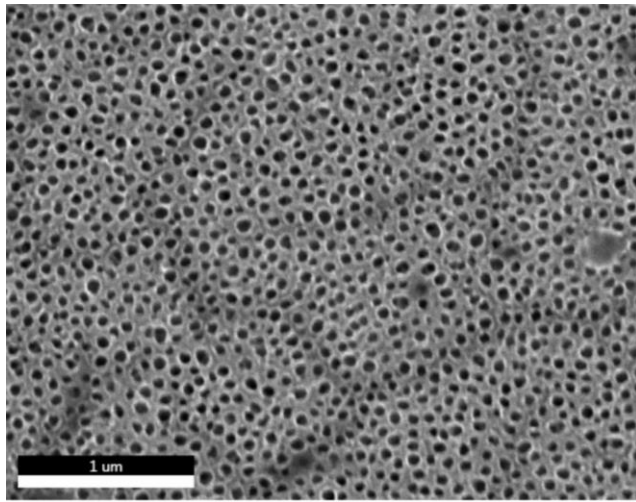
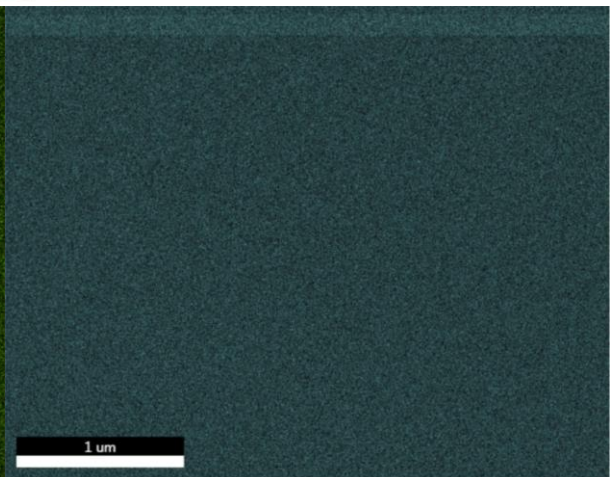
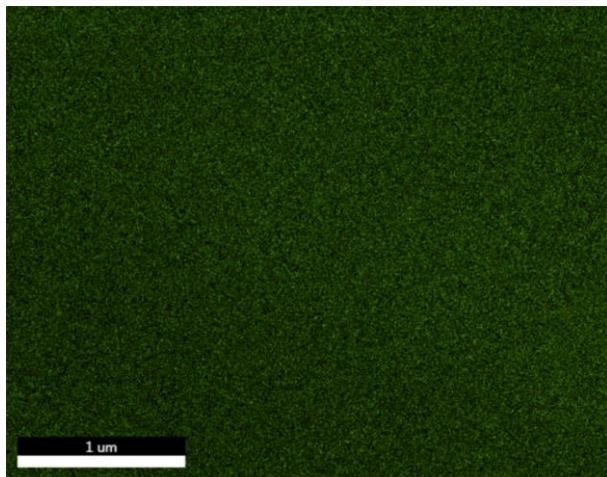


**Fig. S8.** SEM images of nanotube structured Ti/TiO<sub>2</sub> photoanodes

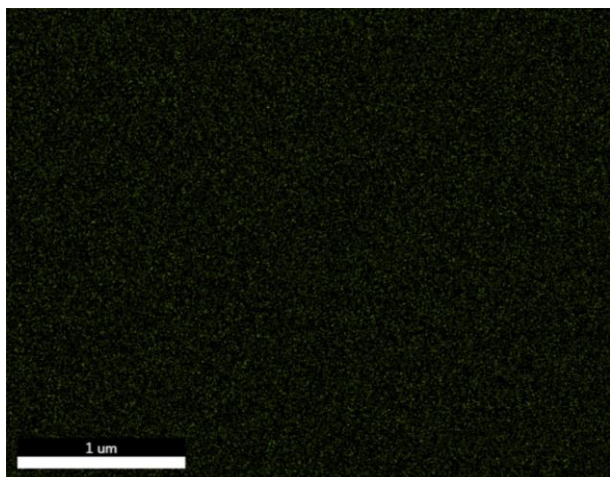


5% O K  
94% Ti K  
1% W L



O K\_ROI (17)

Ti K\_ROI (111)



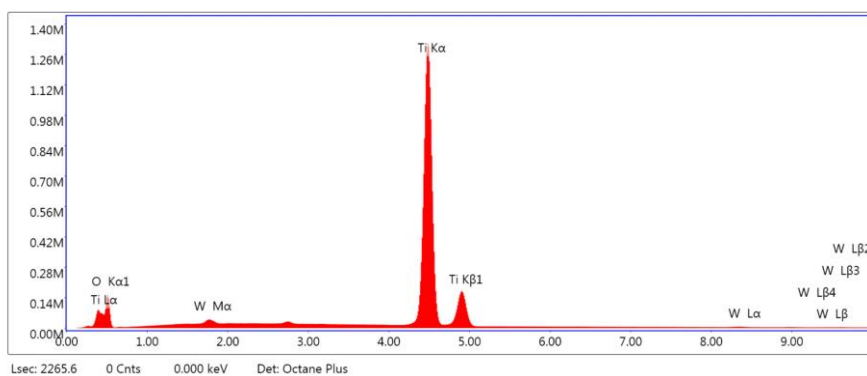
W L\_ROI (8)

## EDAX TEAM

Page

kV:20      Mag:100000      Takeoff: 48.2      Live Time(s): 2265.6      Amp Time(μs): 7.68      Resolution:(e 126  
V) 2

### Sum Spectrum



### eZAF Smart Quant Results

Element	Weight %	Atomic %
O K	23.37	48.05
TiK	75.31	51.71
W L	1.32	0.24

Fig. S9. SEM-EDX mapping results of NT-4h-1WO<sub>3</sub> electrode and its sum spectrum results.

XPS analyses were performed to determine the chemical composition and electronic/valence states of the pristine and W decorated samples (Figs. S10-14). The peaks are indexed at ~37, 284, 459, and 529 eV to the characteristic peaks of W4f, C1s, Ti2p, and O1s (Bhojane & Shirage, 2022). The contribution to the oxygen peak at 529.4 eV corresponds to Ti-O. The other peaks at 531.9 eV and 533.4 eV can be considered due to moisture (or surface hydroxyl groups, H-O) and hydrocarbon (C=O) impurities (Beamson and Briggs1992; Yurdakal et al. 2021). Two bending energy appeared at ~459 and ~464.5 eV attributed to Ti 2p<sub>1/2</sub> (Ti<sup>+4</sup>) and Ti 2p<sub>3/2</sub> (Ti<sup>+4</sup>) (Gao et al. 2016). Two binding energy centered at 36.5 eV (4f<sub>7/2</sub>) and 38.5 eV (4f<sub>5/2</sub>) corresponds to the W<sup>6+</sup> which shows that the decorated W form is WO<sub>3</sub> on the TiO<sub>2</sub> surface (Mahmoud et al. 2022).

The W amount on the TiO<sub>2</sub> surface is very low with respect to those of Ti and O. Therefore, we considered only the prominent peaks (W4f<sub>5/2</sub> and W4f<sub>7/2</sub>) since the others, including the metallic W (at ca. 31-32 eV) (Bera et al., 2012) could be due to baseline noise. Indeed, the WO<sub>3</sub> preparation process is an oxidation reaction in the presence of oxygen, H<sub>2</sub>O<sub>2</sub>, and H<sub>2</sub>SO<sub>4</sub> rather than a reduction.

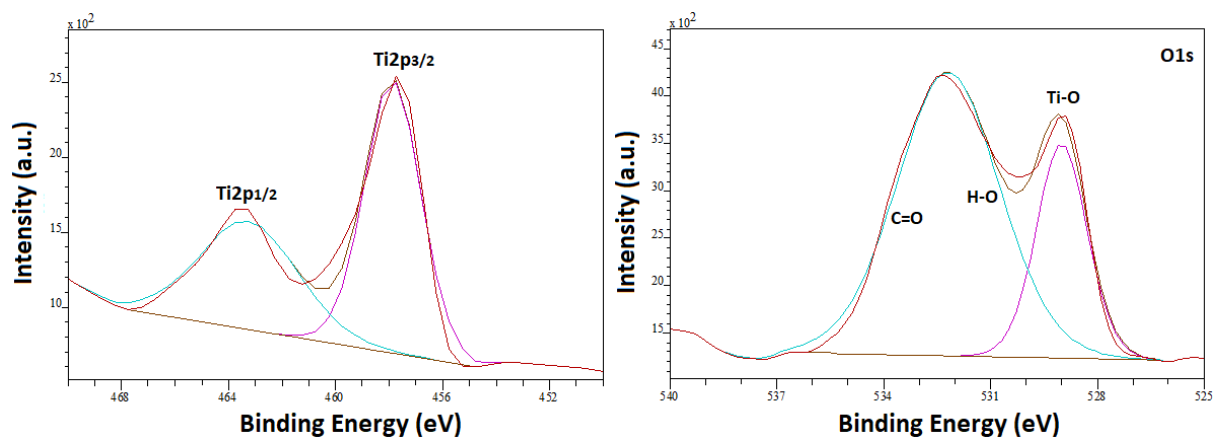


Fig. S10. XPS spectra of NT-4h; (a) Ti 2p, and (b) O 1s

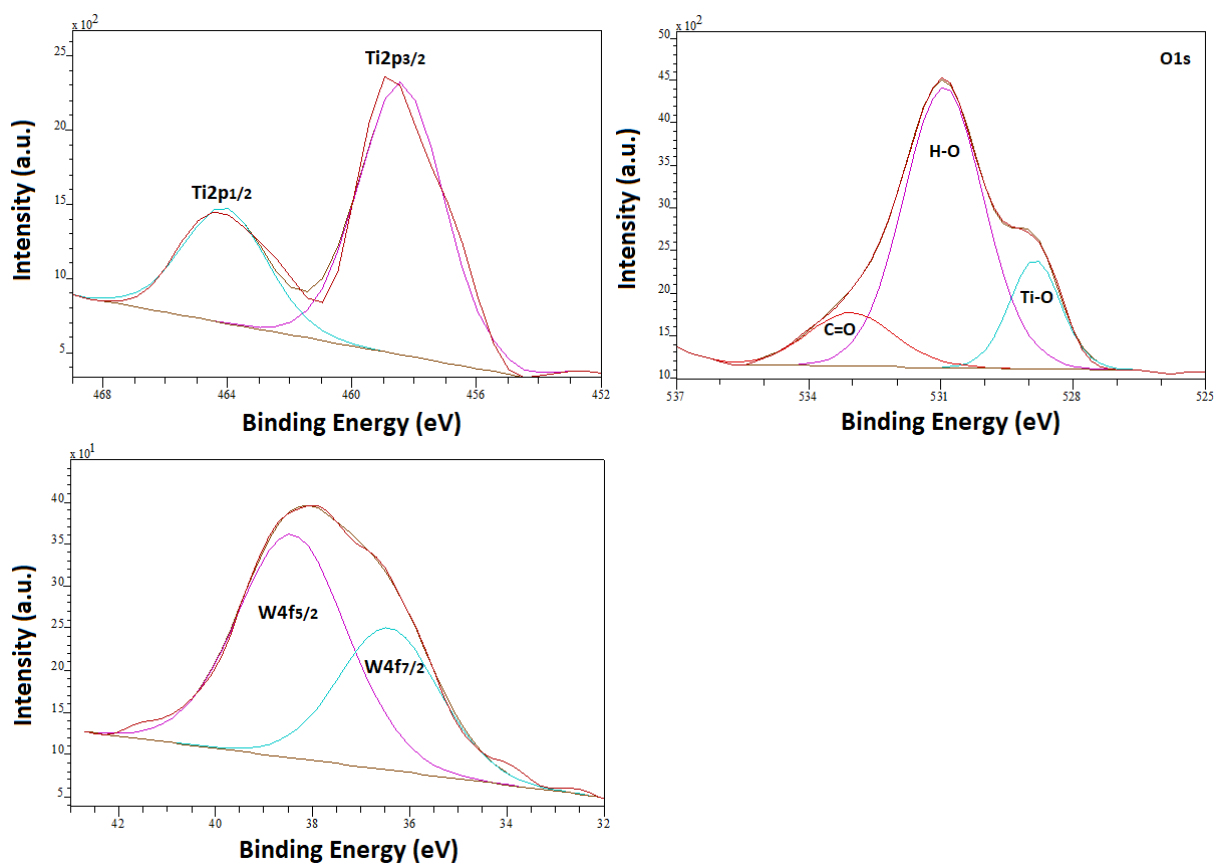


Fig. S11. XPS spectra of NT-4h-1WO<sub>3</sub>; (a) Ti 2p, (b) O 1s, and (c) W 4f.

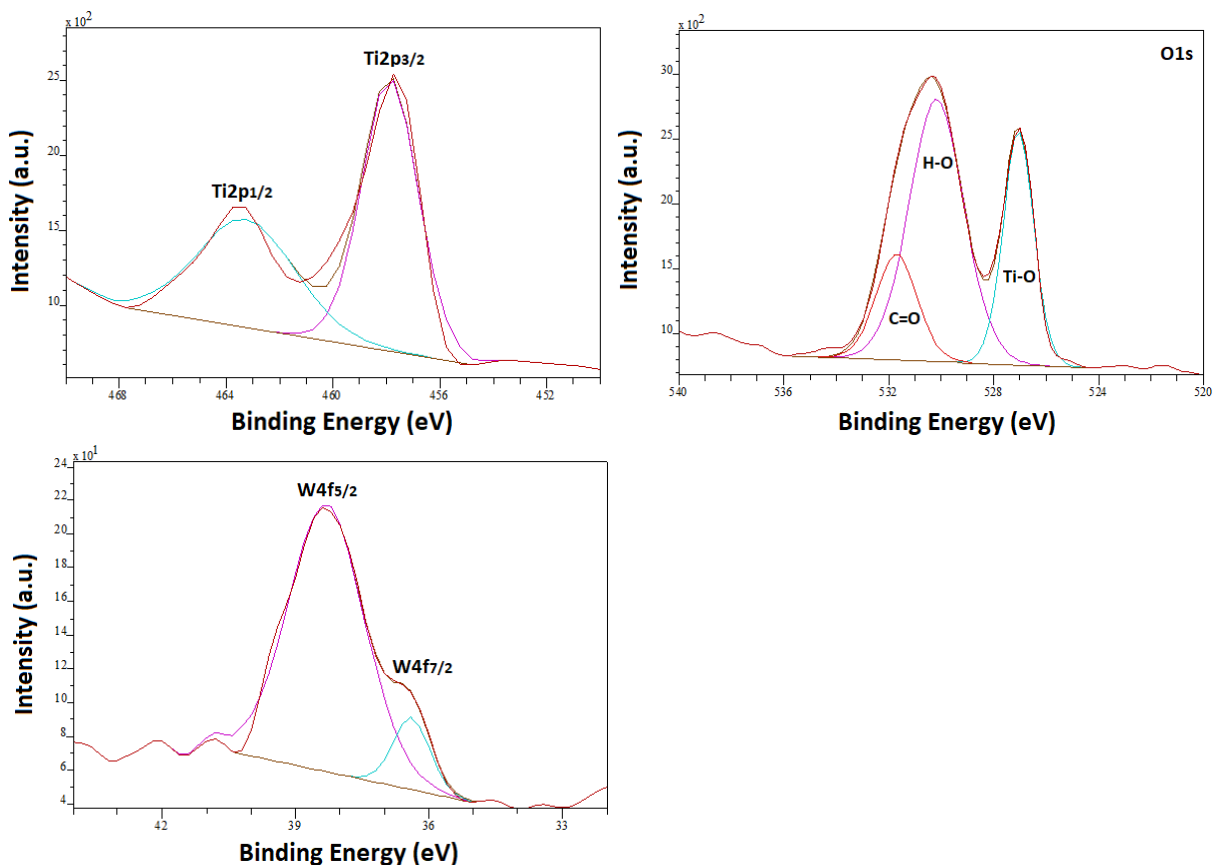


Fig. S12. XPS spectra of NT-4h-0.5WO<sub>3</sub>; (a) Ti 2p, (b) O 1s, and (c) W 4f

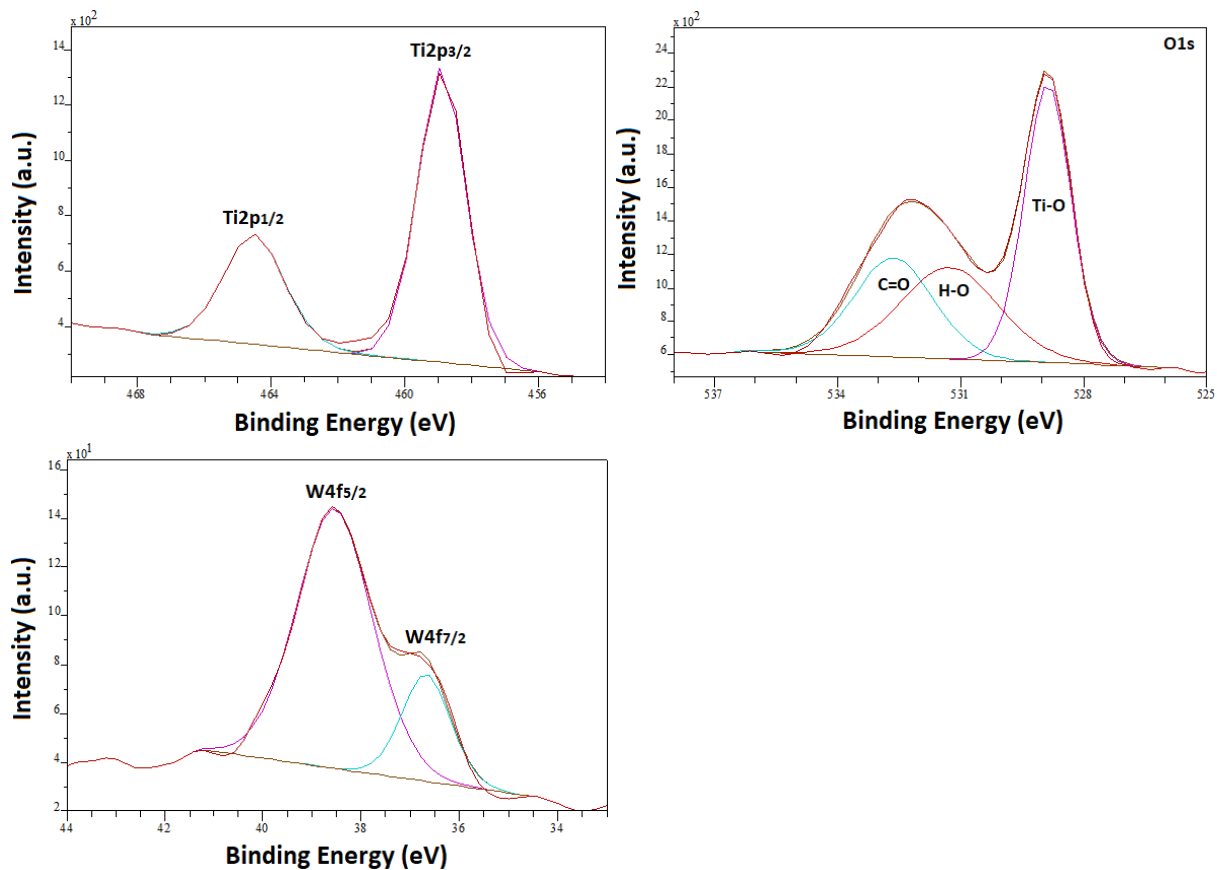
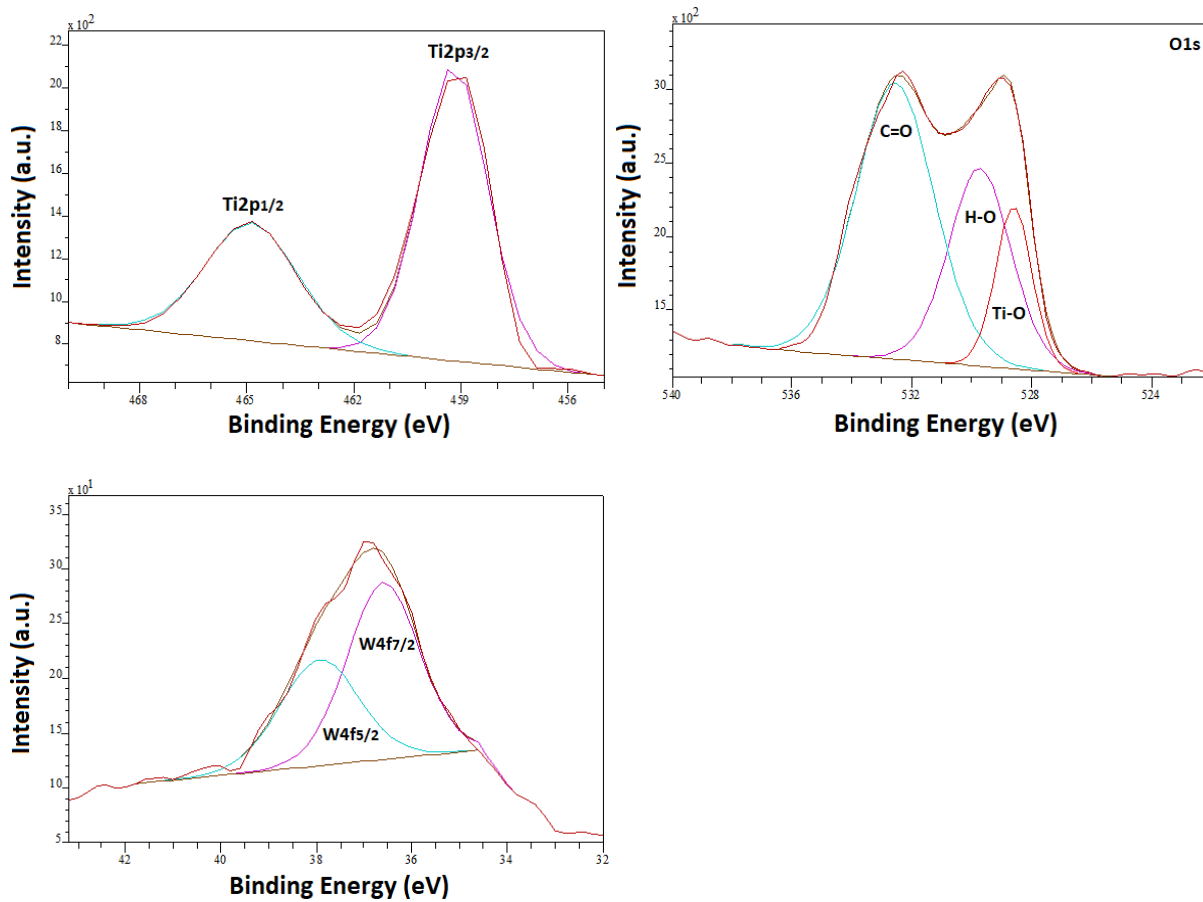


Fig. S13. XPS spectra of NT-4h-1WO<sub>3</sub>-500; (a) Ti 2p, (b) O 1s, and (c) W 4f.



**Fig. S14.** XPS spectra of NT-4h-2WO<sub>3</sub>; (a) Ti 2p, (b) O 1s, and (c) W 4f

Figures S15 and S16 show the (photo)current-potential behaviour of NT-4h and NT-4h-1WO<sub>3</sub> electrodes under UVA (Fig S15) and visible (Fig. S16) irradiations in "5 mM Na<sub>2</sub>SO<sub>4</sub> and 0.50 mM 3-methylpyridine" and "5 mM Na<sub>2</sub>SO<sub>4</sub>". Under dark, virtually no current was obtained using both electrodes. The electrodes showed very high currents under UVA irradiation compared to those observed under visible light. For instance, at 0.5 V, the current under UVA is 80 times (ca. 2000 vs. 25  $\mu$ A) higher than that under Vis light using NT-4h-1WO<sub>3</sub>. In addition, under UVA, the current increased continuously by increasing the potential, while under Vis, a low and constant current was obtained. In addition, a higher current was obtained in the presence of 3-methylpyridine under UVA with respect to its absence. This increase was very noticeable in the presence of the NT-4h-1WO<sub>3</sub> electrode. Indeed, the increase in the presence of 3-methylpyridine with NT-4h-1WO<sub>3</sub> is almost three times higher than that of the NT-4h electrode. In contrast, 3-methylpyridine did not give rise to any current increase under visible irradiation.

The (photo)current behaviour of NT-4h and NT-4h-1WO<sub>3</sub> electrodes under UVA and visible irradiations obtained by a switch on/off of the lamps is shown in Fig. S17. Both electrodes' behaviour is almost overlapped under UVA, and very high and sharp peaks were obtained during switch on/off processes. The photocurrent values at the applied voltage were reached in a very short time, and reproducible results were obtained. Under Vis irradiation, a low current value was obtained, especially with the NT-4h-1WO<sub>3</sub> electrode.

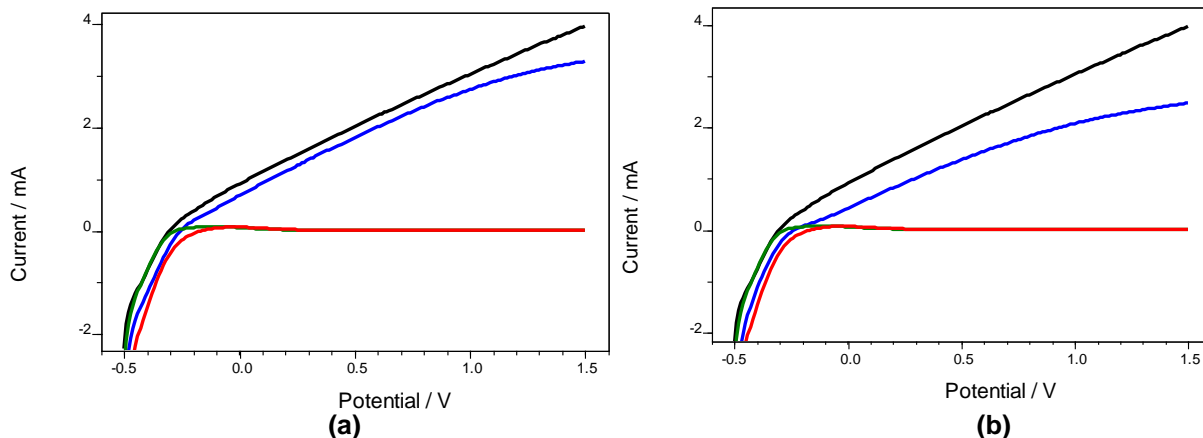


**Fig. S15.** (Photo)current-potential behaviour of NT-4h (a) and NT-4h-1WO<sub>3</sub> (b) electrodes. Measurements were performed under UVA light in “5 mM Na<sub>2</sub>SO<sub>4</sub> and 0.50 mM 3-methylpyridine” (black) and “5 mM Na<sub>2</sub>SO<sub>4</sub>” (blue). The curves in the same conditions but in the dark overlapped (red and green). Reference electrode: Ag/AgCl (3 M KCl). The immersed plate surface area: 25 cm<sup>2</sup>. pH ~7.

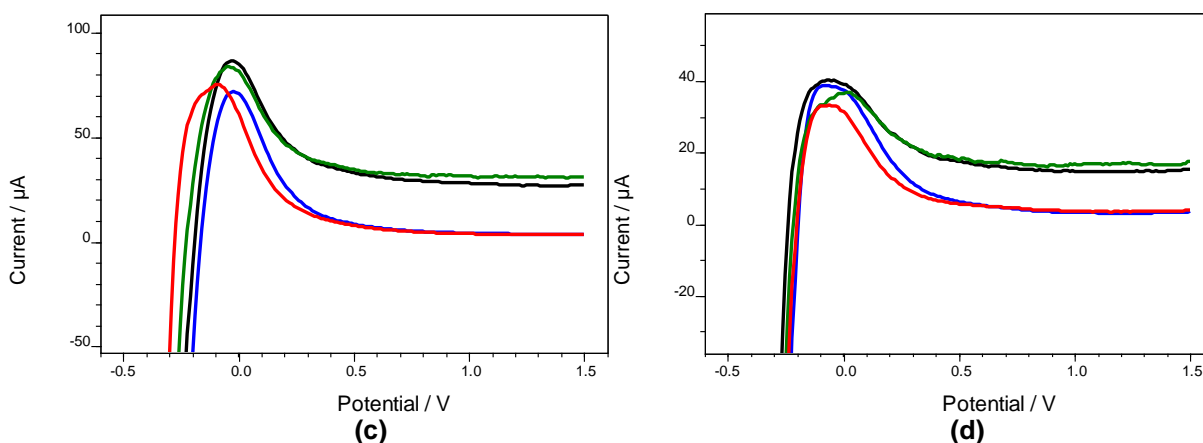


**Fig. S16.** (Photo)current-potential behaviour of NT-4h (a) and NT-4h-1WO<sub>3</sub> (b) electrodes. Measurements were performed under visible light in “5 mM Na<sub>2</sub>SO<sub>4</sub> and 0.50 mM 3-methylpyridine” (black) and “5 mM Na<sub>2</sub>SO<sub>4</sub>” (blue). The curves in the same conditions but in the dark overlapped (red and green). Reference electrode: Ag/AgCl (3 M KCl). The immersed plate surface area: 25 cm<sup>2</sup>. pH ~7.

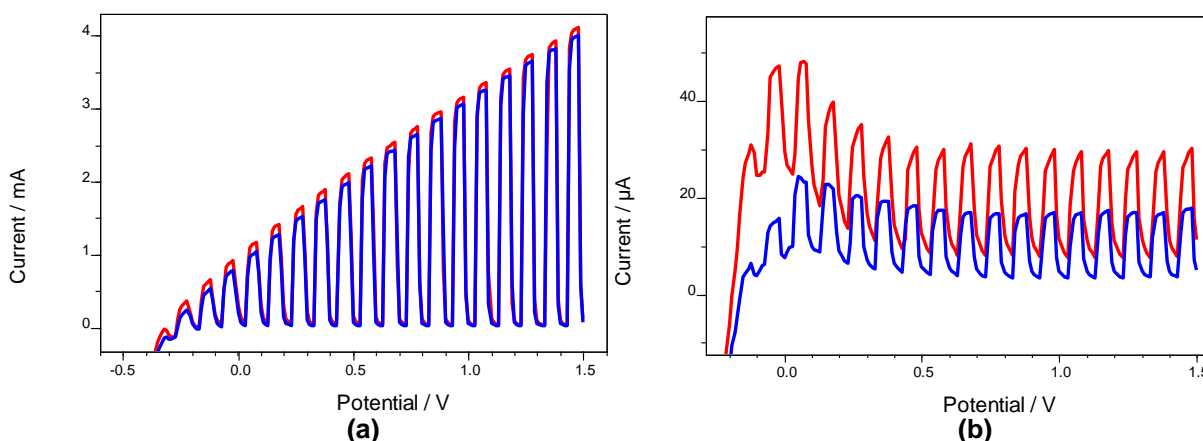


**Fig. S17.** The (photo)current behaviour of NT-4h (red) and NT-4h-1WO<sub>3</sub> (blue) electrodes under UVA (a) and visible (b) irradiations performed in “5 mM Na<sub>2</sub>SO<sub>4</sub> and 0.50 mM 3-methylpyridine”. Each 10 seconds the lamps were switched on or switched off. Reference electrode: Ag/AgCl (3 M KCl). The immersed plate surface area: 25 cm<sup>2</sup>. pH ~7.

**Table S1.** The light intensity values were determined with a radiometer (Deltaohm, DO9721) with probes measuring between 315-400 nm and 400-1050 nm.

Light source	Light intensity, between 315-400 nm (W/m <sup>2</sup> )	Light intensity, between 400-1050 nm (W/m <sup>2</sup> )
UVA	13.95	5.25
Vis	0.156	1212
UVA-Vis	3.01	1170

**Table S2.** The crystalline phases of TiO<sub>2</sub> on Ti plates, peak areas and primary particle sizes of the phases, and average inner diameter and wall thicknesses of the nanotubes. NT: nanotube. A: Anatase; R: Rutile

Electrode	Crystalline phase	Anatase peak area (101)	Rutile peak area (101)	Ti peak area at 2 $\theta$ =40°	Primary particle sizes of A (nm)	Primary particle sizes of R (nm)	Inner diameter of NT (nm)	Wall thicknesses of NT (nm)
NT-15min	A	100	-	1028	30.0		30	23
NT-30min	A + trace R	278	11.5	1068	27.3	25.4	35	20
NT-1h	A + trace R	486	33.0	1043	27.9	21.8	40	15
NT-2h	A + trace R	331	9.2	870	28.2	30.6	50	15
NT-3h	A + trace R	613	23.3	1115	27.5	51.8	50	14
NT-4h	A + trace R	1520	22.0	500	27.5	22.3	50	14
NT-5h	A + trace R	698	20.9	1200	27.3	36.5	50	10

**Table S3.** The experimental results of PEC oxidation of 3-methylpyridine (0.5 mM) by nanotube structured Ti/TiO<sub>2</sub> electrodes prepared by anodic oxidation method for different times. Initial pH = 7, Potential: 0.5 V, [Na<sub>2</sub>SO<sub>4</sub>]: 5 mM, light source: UVA.

Electrode	$-r_0 \times 10^3$ (mM h <sup>-1</sup> )	$k \times 10^3$ (h <sup>-1</sup> )	<sup>a</sup> S <sub>3</sub> -Pyridinemethanol		<sup>b</sup> S <sub>3</sub> -Pyridinemethanal		<sup>c</sup> S <sub>Vitamin B3</sub>		X <sub>1h</sub> (%)	X <sub>3h</sub> (%)	<sup>d</sup> S <sub>CO<sub>2</sub>/6</sub> (%)	<sup>e</sup> pH
			1h (%)	3h (%)	1h (%)	3h (%)	1h (%)	3h (%)				
NT-15min	59.6	89.3	4	4	10	9	10	8	10	24	36	6.58
NT-30min	78.2	115	4	4	11	9	8	7	13	30	45	6.48
NT-1h	87.7	140	4	4	11	10	9	8	16	35	37	6.46
NT-2h	91.4	142	5	4	12	10	9	8	16	36	44	6.33
NT-3h	103	146	5	5	12	11	11	10	16	36	38	6.16
NT-4h	126	168	5	4	11	10	9	9	19	40	48	6.13
NT-5h	86.6	169	5	4	11	9	11	11	17	40	47	6.09

$-r_0$ : initial reaction rate,  $k$ : first order rate constant. <sup>a</sup>S<sub>3</sub>-Pyridinemethanol, <sup>b</sup>S<sub>3</sub>-Pyridinemethanal and <sup>c</sup>S<sub>Vitamin B3</sub>: 3-pyridinemethanol, 3-pyridinemethanal and vitamin B<sub>3</sub> selectivity's after 1h and 3h conversions. X<sub>1h</sub> and X<sub>3h</sub>: the conversion values after 1h and 3h of reaction times, respectively. <sup>d</sup>CO<sub>2</sub>/6 selectivity was divided by 6 for stoichiometric normalization and considered after 3h of reaction time. <sup>e</sup>pH: solution pH value at the end of the experiment.

**Table S4.** The experimental results of photoelectrocatalytic oxidation of 3-methylpyridine (0.5 mM) by NT-4h-1WO<sub>3</sub> electrode for different potential and Na<sub>2</sub>SO<sub>4</sub> concentration values. pH 7, light source: **UVA**.

Bias (V)	Na <sub>2</sub> SO <sub>4</sub> (mM)	-r <sub>0</sub> × 10 <sup>3</sup> (mM h <sup>-1</sup> )	k × 10 <sup>3</sup> (h <sup>-1</sup> )	<sup>a</sup> S <sub>3</sub> -Pyridinemethanol		<sup>b</sup> S <sub>3</sub> -Pyridinemethanal		<sup>c</sup> S <sub>Vitamin B3</sub>		X <sub>1h</sub> (%)	X <sub>3h</sub> (%)	<sup>d</sup> S <sub>CO<sub>2</sub>/6</sub> for X <sub>3h</sub> (%)	°pH
				1h (%)	3h (%)	1h (%)	3h (%)	1h (%)	3h (%)				
0.25	5	177	486	8	3	22	12	32	48	33	77	14	4.93
<b>0.50</b>	<b>5</b>	221	613	6	2	19	8	34	51	<b>39</b>	<b>85</b>	15	4.63
0.75	5	202	596	5	1	16	6	37	49	<b>38</b>	<b>84</b>	15	4.62
1.0	5	229	665	5	1	13	5	36	46	<b>41</b>	<b>87</b>	18	4.44
1.5	5	237	591	6	4	10	2	38	43	<b>42</b>	<b>83</b>	20	4.72
0.5	2.5	185	544	8	2	26	13	30	51	<b>38</b>	<b>80</b>	11	4.78
0.5	10	210	581	5	2	14	6	34	45	<b>39</b>	<b>83</b>	19	4.61

-r<sub>0</sub>: initial reaction rate, k: first order rate constant. <sup>a</sup>S<sub>3</sub>-Pyridinemethanol, <sup>b</sup>S<sub>3</sub>-Pyridinemethanal and <sup>c</sup>S<sub>Vitamin B3</sub>: 3-pyridinemethanol, 3-pyridinemethanal and vitamin B<sub>3</sub> selectivity's after 1h and 3h conversions. X<sub>1h</sub> and X<sub>3h</sub>: the conversion values after 1h and 3h of reaction times, respectively. <sup>d</sup>CO<sub>2</sub>/6 selectivity was divided by 6 for stoichiometric normalization and considered after 3h of reaction time. °pH: solution pH value at the end of the experiment.

**Table S5.** The experimental results of PEC, oxidation of 3-methylpyridine (0.5 mM) by NT-4h and NT-4h-1WO<sub>3</sub> electrode, and EC and PC oxidations by NT-4h-1WO<sub>3</sub>. Initial pH = 7, light source: **Visible irradiation**.

Electrode		-r <sub>0</sub> × 10 <sup>3</sup> (mM h <sup>-1</sup> )	k × 10 <sup>3</sup> (h <sup>-1</sup> )	<sup>a</sup> S <sub>3</sub> -Pyridinemethanol		<sup>b</sup> S <sub>3</sub> -Pyridinemethanal		<sup>c</sup> S <sub>Vitamin B3</sub>		X <sub>1h</sub> (%)	X <sub>3h</sub> (%)	<sup>d</sup> S <sub>CO<sub>2</sub>/6</sub> (%)	°pH
				1h (%)	3h (%)	1h (%)	3h (%)	1h (%)	3h (%)				
NT-4h	PEC	11.9	57.1	0	0	0.3	0.4	4	1	<b>3</b>	<b>16</b>	66	6.82
NT-4h-1WO <sub>3</sub>	PEC	27.4	105	0	0	2	1	0	0	<b>7</b>	<b>28</b>	100	6.90
NT-4h-1WO <sub>3</sub> -500	PEC	35.5	104	0	0	1	1	0	0	<b>7</b>	<b>27</b>	100	6.97
NT-4h-0.5WO <sub>3</sub>	PEC	23.6	58.7	0	0	1	1	0	0	<b>4</b>	<b>17</b>	100	6.92
NT-4h-2WO <sub>3</sub>	PEC	21.8	58.4	0	0	1	0.4	0	0	<b>3</b>	<b>16</b>	100	6.90
NT-4h-1WO <sub>3</sub>	PC	39.3	73.5	0	0	0	0.2	0	0	<b>6</b>	<b>20</b>	100	6.92
NT-4h-1WO <sub>3</sub>	EC	2.22	7.98	0	0	0	0	0	0	<b>1</b>	<b>3</b>		6.83

-r<sub>0</sub>: initial reaction rate, k: first order rate constant. <sup>a</sup>S<sub>3</sub>-Pyridinemethanol, <sup>b</sup>S<sub>3</sub>-Pyridinemethanal and <sup>c</sup>S<sub>Vitamin B3</sub>: 3-pyridinemethanol, 3-pyridinemethanal and vitamin B<sub>3</sub> selectivity's after 1h and 3h conversions. X<sub>1h</sub> and X<sub>3h</sub>: the conversion values after 1h and 3h of reaction times, respectively. <sup>d</sup>CO<sub>2</sub>/6 selectivity was divided by 6 for stoichiometric normalization and considered after 3h of reaction time. °pH: solution pH value at the end of the experiment.

**Table S6.** The experimental results of photolytic oxidation of 3-methylpyridine (0.5 mM). pH 7. [Na<sub>2</sub>SO<sub>4</sub>]: 5 mM.

Substrate	Irradiation	-r <sub>0</sub> × 10 <sup>3</sup> (mM h <sup>-1</sup> )	k × 10 <sup>3</sup> (h <sup>-1</sup> )	<sup>a</sup> S <sub>3</sub> -Pyridinemethanol		<sup>b</sup> S <sub>3</sub> -Pyridinemethanal		<sup>c</sup> S <sub>Vitamin B3</sub>		X <sub>1h</sub> (%)	X <sub>3h</sub> (%)	<sup>d</sup> S <sub>CO<sub>2</sub>/6</sub> (%)	°pH
				1h (%)	3h (%)	1h (%)	3h (%)	1h (%)	3h (%)				
3-methylpyridine	VIS	5.58	57.1	0	0	0	0	0	0	<b>3</b>	<b>16</b>	100	7
3-methylpyridine	UVA	22.3	47.0	0	0	0	0	0	0	<b>4</b>	<b>13</b>	100	7
3-pyridinemethanol	VIS	0	0	0	0	0	0	0	0	0	0	0	7
3-pyridinemethanol	UVA	0	0	0	0	0	0	0	0	0	0	0	7

-r<sub>0</sub>: initial reaction rate, k: first order rate constant. <sup>a</sup>S<sub>3</sub>-Pyridinemethanol, <sup>b</sup>S<sub>3</sub>-Pyridinemethanal and <sup>c</sup>S<sub>Vitamin B3</sub>: 3-pyridinemethanol, 3-pyridinemethanal and vitamin B<sub>3</sub> selectivity's after 1h and 3h conversions. X<sub>1h</sub> and X<sub>3h</sub>: the conversion values after 1h and 3h of reaction times, respectively. <sup>d</sup>CO<sub>2</sub>/6 selectivity was divided by 6 for stoichiometric normalization and considered after 3h of reaction time. °pH: solution pH value at the end of the experiment.

**Table S7.** The experimental results of PEC oxidation of 3-methylpyridine (0.5 mM) by NT-4h-1WO<sub>3</sub> electrode. Initial pH = 7, light source: **UV-Visible** irradiation.

Electrode	$-r_0 \times 10^3$ (mM h <sup>-1</sup> )	$k \times 10^3$ (h <sup>-1</sup> )	<sup>a</sup> S <sub>3-Pyridinemethanol</sub>		<sup>b</sup> S <sub>3-Pyridinemethanal</sub>		<sup>c</sup> S <sub>Vitamin B3</sub>		X <sub>1h</sub> (%)	X <sub>3h</sub> (%)	<sup>d</sup> S <sub>CO<sub>2</sub>/6</sub> (%)	<sup>e</sup> pH
			1h (%)	3h (%)	1h (%)	3h (%)	1h (%)	3h (%)				
NT-4h-0.5WO <sub>3</sub>	78.7	192	9	8	21	18	7	8	15	44	40	6.63
NT-4h-1WO <sub>3</sub>	202	586	5	2	18	10	24	37	37	83	23	4.80
NT-4h-1WO <sub>3</sub> -500	131	290	7	6	20	16	12	13	24	59	37	6.19
NT-4h-2WO <sub>3</sub>	71.9	194	10	8	19	18	6	7	14	45	38	6.68

$-r_0$ : initial reaction rate, k: first order rate constant. <sup>a</sup>S<sub>3-Pyridinemethanol</sub>, <sup>b</sup>S<sub>3-Pyridinemethanal</sub> and <sup>c</sup>S<sub>Vitamin B3</sub>: 3-pyridinemethanol, 3-pyridinemethanal and vitamin B<sub>3</sub> selectivity's after 1h and 3h conversions. X<sub>1h</sub> and X<sub>3h</sub>: the conversion values after 1h and 3h of reaction times, respectively. <sup>d</sup>CO<sub>2</sub>/6 selectivity was divided by 6 for stoichiometric normalization and considered after 3h of reaction time. <sup>e</sup>pH: solution pH value at the end of the experiment.

**Table S8.** The experimental results of PEC oxidation of different substrates (0.5 mM) by NT-4h-1WO<sub>3</sub> electrode under UVA or Visible irradiations. Initial pH = 7, Potential: 0.5 V, [Na<sub>2</sub>SO<sub>4</sub>]: 5 mM.

Substrate	Light source	$-r_0 \times 10^3$ (mM h <sup>-1</sup> )	$k \times 10^3$ (h <sup>-1</sup> )	<sup>a</sup> S <sub>3-Pyridinemethanol</sub>		<sup>b</sup> S <sub>3-Pyridinemethanal</sub>		<sup>c</sup> S <sub>Vitamin B3</sub>		X <sub>1h</sub> (%)	X <sub>3h</sub> (%)	<sup>d</sup> S <sub>CO<sub>2</sub>/6</sub> (%)	<sup>e</sup> pH
				1h (%)	3h (%)	1h (%)	3h (%)	1h (%)	3h (%)				
3-methylpyridine	UVA	221	613	6	2	19	8	34	51	39	85	15	4.63
3-methylpyridine	Vis	27.4	105	0	0	2	1	0	0	7	28	100	6.90
3-pyridinemethanol	UVA	207	639			54	25	42	66	40	86	5.8	4.55
3-pyridinemethanol	Vis	0	0			0	0	0	0	0	0		7
3-pyridinemethanal	UVA	192	546					94	86	38	81	13	4.26
3-pyridinemethanal	Vis	0	0					0	0	0	0		7
vitamin B <sub>3</sub>	UVA	50.6	77.5							8	22	48	4.12
vitamin B <sub>3</sub>	Vis	0	0							0	0		7

$-r_0$ : initial reaction rate, k: first order rate constant. <sup>a</sup>S<sub>3-Pyridinemethanol</sub>, <sup>b</sup>S<sub>3-Pyridinemethanal</sub> and <sup>c</sup>S<sub>Vitamin B3</sub>: 3-pyridinemethanol, 3-pyridinemethanal and vitamin B<sub>3</sub> selectivity's after 1h and 3h conversions. X<sub>1h</sub> and X<sub>3h</sub>: the conversion values after 1h and 3h of reaction times, respectively. <sup>d</sup>CO<sub>2</sub>/6 selectivity was divided by 6 for stoichiometric normalization and considered after 3h of reaction time. <sup>e</sup>pH: solution pH value at the end of the experiment.

## Acknowledgements

Authors thank TÜBİTAK (Project no: 221Z085) for financial support, Assoc. Prof. Dr. Özer Gök (Eskişehir Technical University, Turkey) for XPS, Eng. Mehmet Akkaş (ILTEM, University of Kütahya Dumlupınar, Turkey) for the SEM-EDX and Eng. Hakan Şahin (TUAM, University of Afyon Kocatepe, Turkey) for the XRD analyses.

## References

- Amin, V.M., Olson, N.F., Spectrophotometric determination of hydrogen peroxide in milk, *Journal of Dairy Science*, 50 (1967) 461-464.
- Beamson, G., Briggs, D. High Resolution XPS of Organic Polymers, The Scienta ESCA300 Database, 1st edn, Wiley Interscience, 1992.
- Bera, P., Seenivasan, H., Rajam, K.S., William Grips V.K., XRD, FESEM and XPS studies on heat treated Co–W electrodeposits, *Mater. Lett.*, 76 (2012) 103-105.
- Bhojane, P., Shirage, P.M. Facile preparation of hexagonal WO<sub>3</sub> nanopillars and its reduced graphene oxide nanocomposites for high-performance supercapacitor, *J. Energy Storage*, 55 (2022) 105649.
- Çetinkaya, S., Khamidov, G., Özcan, L., Palmisano, L., Yurdakal, S., Selective photoelectrocatalytic oxidation of glycerol by nanotube, nanobelt and nanosponge structured TiO<sub>2</sub> on Ti plates, *J. Envir. Chem. Eng.*, 10 (2022) 107210.
- Davaslıoğlu, İ.Ç., Özdokur, K.V., Koçak, S., Çırak, Ç., Çağlar, B., Çırak, B.B., Ertaş, F.N., WO<sub>3</sub> Decorated TiO<sub>2</sub> Nanotube Array Electrode: Preparation, Characterization and Superior Photoelectrochemical Performance for Rhodamine B Dye Degradation, *J. Mol. Struct.*, 1241 (2021) 130673.
- Gao, L. et al. Negative oxygen ions production by superamphiphobic and antibacterial TiO<sub>2</sub>/Cu<sub>2</sub>O composite film anchored on wooden substrates. *Sci. Rep.* 6 (2016) 26055–26064.
- Gökdere, B., Üzer, A., Durmazel, S., Erçağ, E., Apak, R., Titanium dioxide nanoparticles–based colorimetric sensors for determination of hydrogen peroxide and triacetone triperoxide (TATP), *Talanta*, 202, 2019, 402-410.
- Mahmoud, Z.H., AL-Bayati, R.A., Khadom, A.A. Modified anatase phase of TiO<sub>2</sub> by WO<sub>3</sub> nanoparticles: Structural, morphology and spectral evaluations, *Mater. Today: Proc.*, 61 (2022) 799-804.
- Martins, A.S., Cordeiro-Junior, P.J M., Nuñez, L., de Vasconcelos Lanza, M.R. A Simple Method for the Electrodeposition of WO<sub>3</sub> in TiO<sub>2</sub> Nanotubes: Influence of the Amount of Tungsten on Photoelectrocatalytic Activity, *Electrocatalysis* (2017) 8:115–121.
- Yurdakal, S., Çetinkaya, S., Şarлак, M. B., Özcan, L., Loddo, V., Palmisano, L. Photoelectrocatalytic oxidation of 3-pyridinemethanol to 3-pyridinemethanal and vitamin B<sub>3</sub> by TiO<sub>2</sub> nanotubes, *Catal. Sci. Technol.*, 10 (2020) 124-137.
- Yurdakal, S., Çetinkaya, S., Özcan, L., Gök, Ö., Palmisano, L., Partial photoelectrocatalytic oxidation of 3-pyridinemethanol by Pt, Au and Pd loaded TiO<sub>2</sub> nanotubes on Ti plate, *Catal. Today*, 380, (2021) 248-258.